Multiple nuclear-replicating viruses require the stress-induced protein ZC3H11A for efficient growth

Shady Younis[a,b,1], Wael Kamel[a,1], Tina Falkeborn[c], Hao Wang[d], Di Yu[e], Robert Daniels[d], Magnus Essand[e], Jorma Hinkula[c], Göran Akusjärvi[a,2], and Leif Andersson[a,f,g,2]

[a]Department of Medical Biochemistry and Microbiology, Uppsala University, SE-751 23 Uppsala, Sweden; [b]Department of Animal Production, Ain Shams University, Shoubra El-Kheima, 11241 Cairo, Egypt; [c]Department of Clinical and Experimental Medicine, Linköping University, SE-58183 Linköping, Sweden; [d]Department of Biochemistry and Biophysics, Stockholm University, SE-10691 Stockholm, Sweden; [e]Department of Immunology, Genetics and Pathology, Uppsala University, SE-751 23 Uppsala, Sweden; [f]Department of Animal Breeding and Genetics, Swedish University of Agricultural Sciences, SE-75007 Uppsala, Sweden; and [g]Department of Veterinary Integrative Biosciences, Texas A&M University, College Station, TX 77483

Contributed by Leif Andersson, February 22, 2018 (sent for review December 22, 2017; reviewed by Phillip A. Sharp and Joan A. Steitz)

The zinc finger CCCH-type containing 11A (*ZC3H11A*) gene encodes a well-conserved zinc finger protein that may function in mRNA export as it has been shown to associate with the transcription export (TREX) complex in proteomic screens. Here, we report that ZC3H11A is a stress-induced nuclear protein with RNA-binding capacity that localizes to nuclear splicing speckles. During an adenovirus infection, the ZC3H11A protein and splicing factor SRSF2 relocalize to nuclear regions where viral DNA replication and transcription take place. Knockout (KO) of *ZC3H11A* in HeLa cells demonstrated that several nuclear-replicating viruses are dependent on ZC3H11A for efficient growth (HIV, influenza virus, herpes simplex virus, and adenovirus), whereas cytoplasmic replicating viruses are not (vaccinia virus and Semliki Forest virus). High-throughput sequencing of ZC3H11A–cross-linked RNA showed that ZC3H11A binds to short purine-rich ribonucleotide stretches in cellular and adenoviral transcripts. We show that the RNA-binding property of ZC3H11A is crucial for its function and localization. In ZC3H11A KO cells, the adenovirus fiber mRNA accumulates in the cell nucleus. Our results suggest that ZC3H11A is important for maintaining nuclear export of mRNAs during stress and that several nuclear-replicating viruses take advantage of this mechanism to facilitate their replication.

ZC3H11A | mRNA export | stress response | virus infection

Zinc finger CCCH-type containing 11A (ZC3H11A) is a poorly characterized zinc finger protein present in all vertebrates. The *ZC3H11A* gene harbors another zinc finger protein gene, *ZBED6*, in one of its introns (Fig. 1*A*). *ZBED6* has evolved from a domesticated DNA transposon and is unique to placental mammals. It encodes a transcription factor that acts as a repressor of the insulin-like growth factor 2 (*IGF2*) gene (1–3). Zinc finger protein genes are one of the largest multigene families in eukaryotes. ZC3H11A contains three tandem CCCH zinc finger domains and belongs to a subfamily of zinc finger proteins that are largely uncharacterized (4). Zinc finger proteins are involved in essential molecular processes such as gene transcription, translation, mRNA processing, protein folding, and chromatin remodeling. Recent proteomic reports have indicated that ZC3H11A may be a component of the transcription export (TREX) complex (5, 6). The TREX complex is conserved from yeast to humans and serves a function in mRNA export (7).

The TREX complex has an integrating role in gene expression by linking multiple mRNA processing steps with mRNA export. Thus, TREX proteins make physical interactions with the 5′ cap-binding complex and the exon junction complex, which is deposited at each splice junction following the catalytic steps of splicing. Further, the TREX complex serves a function in polyadenylation of mRNAs by associating with 3′ end processing factors. The TREX complex consists of a stable subcomplex called THO and multiple additional factors, including ALYREF, UAP56, and ZC3H11A (8). ALYREF serves an important function by recruiting NXF1 to TREX and handing over the mRNA to NXF1 for transport through the nuclear pore complex. In human cells, recruitment of the TREX complex to pre-mRNA is splicing-dependent, possibly because the UAP65 component of the TREX complex binds U2AF-65K, which is necessary for 3′ splice site recognition during spliceosome assembly (9, 10). Interestingly, individual TREX complex components appear to be required for export of distinct subsets of mRNAs. Knockdown of *ZC3H11A* by RNAi has been suggested to lead to nuclear accumulation of total polyA$^+$ mRNA in HeLa cells, a result that suggests that ZC3H11A indeed is required for nuclear-to-cytoplasmic mRNA export (11).

Here, we have inactivated *ZC3H11A* in HeLa cells using the CRISPR/Cas9 system to further study its function in normal cells and under stress conditions. We show that ZC3H11A is superfluous for HeLa cell growth but required for efficient replication of human viruses with a nuclear replication cycle.

Results

ZC3H11A Is Dispensable for HeLa Cell Survival but Required for Efficient Growth of Human Adenovirus. We used CRISPR/Cas9 to inactivate *ZC3H11A* in HeLa cells. The guide RNA (gRNA) was designed to target the second coding exon in *ZC3H11A* (Fig. 1*A* and Fig. S1 *A* and *B*). Three individual clones with a complete

Significance

There is a strong need for the development of new antiviral therapies, and this study sheds light on a host–virus interaction that is significant for a number of medically important human viruses. The study also suggests that the RNA-binding zinc finger CCCH-type containing 11A (ZC3H11A) protein takes part in a mechanism that facilitates nuclear export of mRNA, particularly under cellular stress, a mechanism that has been "hijacked" by several nuclear-replicating viruses to promote their replication. ZC3H11A is therefore a potential target for development of an antiviral therapy.

Author contributions: S.Y., W.K., G.A., and L.A. designed research; S.Y., W.K., T.F., H.W., and D.Y. performed research; S.Y., W.K., T.F., H.W., D.Y., R.D., M.E., J.H., G.A., and L.A. analyzed data; and S.Y., W.K., G.A., and L.A. wrote the paper.

Reviewers: P.A.S., Massachusetts Institute of Technology; and J.A.S., Yale University/Howard Hughes Medical Institute.

Conflict of interest statement: S.Y., W.K., G.A., and L.A. are coauthors on a patent application filed based on some of the results in this study.

Data deposition: The RNA-seq data have been deposited in the NCBI Sequence Read Archive (accession no. SRP133853).

[1]S.Y. and W.K. contributed equally to this work.

[2]To whom correspondence may be addressed. Email: goran.akusjarvi@imbim.uu.se or leif.andersson@imbim.uu.se.

This article contains supporting information online at www.pnas.org/lookup/suppl/doi:10.1073/pnas.1722333115/-/DCSupplemental.

Published online April 2, 2018.

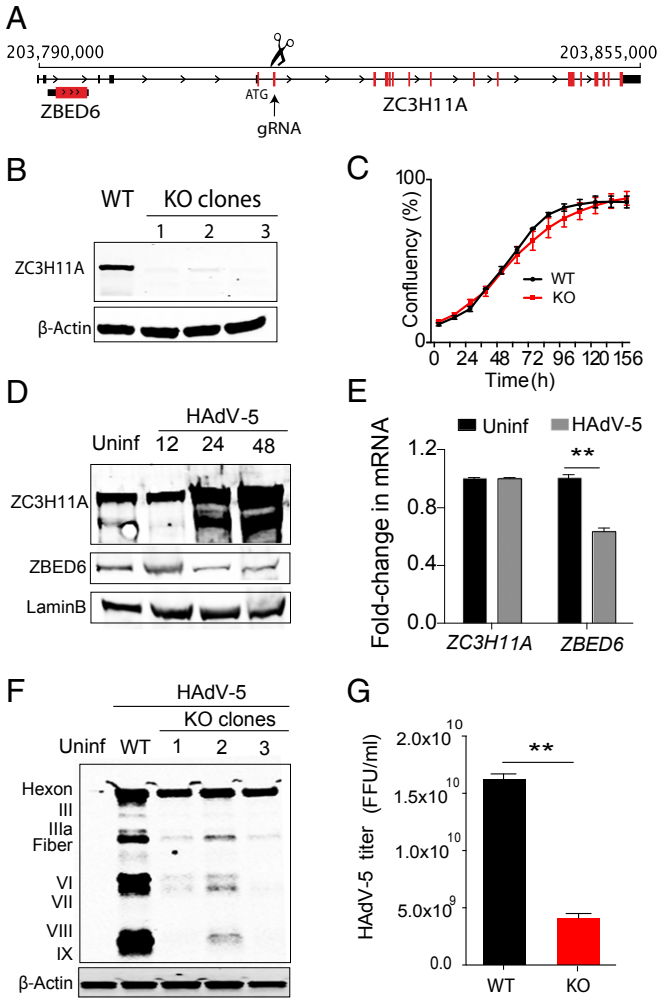

Fig. 1. KO of *ZC3H11A* in human HeLa cells inhibits adenovirus growth. (*A*) Schematic description of the *ZC3H11A* targeting strategy using CRISPR/Cas9. The gRNA arrow indicates the targeted exon. Black and red vertical lines represent the noncoding (UTRs) and coding parts of the transcript, respectively. (*B*) Immunoblot validation of three ZC3H11A-KO clones. (*C*) Real-time measurements of cell growth (mean ± SEM) for parental (black) and ZC3H11A-KO (red) cells ($n = 3$). (*D*) Immunoblot detection of ZC3H11A, ZBED6, and LaminB (loading control) during HAdV-5 virus infection of WT cells. (*E*) Quantitative PCR analysis of *ZC3H11A* and *ZBED6* mRNA expression levels before and after HAdV-5 infection. $^{**}P < 0.01$. (*F*) Immunoblot analysis of HAdV-5 capsid protein expression in WT and the three ZC3H11A-KO clones. (*G*) HAdV-5 titer in WT and ZC3H11A-KO cells. Uninf, uninfected cells subjected to the same treatment as infected cells. $^{**}P < 0.01$.

loss of ZC3H11A protein expression were isolated (Fig. 1*B*). The mutations introduced into the three clones were characterized by DNA sequencing (Fig. S1*C*). The sequencing results show that clones 2 and 3 are identical, with an insertion of the same random nucleotides. The *ZC3H11A* knockout (KO) cells grow essentially as wild-type (WT) cells without any obvious phenotypic changes or large effects on growth kinetics (Fig. 1*C*), suggesting that ZC3H11A function is not essential for HeLa cell growth.

To explore the function of the ZCH311A protein under stress conditions, we infected the *ZC3H11A* KO and WT cells with human adenovirus type 5 (HAdV-5). Interestingly, the infection resulted in a significant increase in the steady-state amount of the ZC3H11A protein at late time points of infection (Fig. 1*D*). This was unexpected since adenovirus efficiently shuts down host cell protein synthesis during the late stage of infection (12). The increase of ZC3H11A protein expression during virus infection was not accompanied by an increase in the *ZC3H11A* transcript abundance (Fig. 1*E*). Since HAdV-5 blocks host cell mRNA translation by inhibiting cap-dependent translation initiation, the results suggest that the virus infection most likely enhanced ZC3H11A protein expression at the level of protein stability. ZBED6, which is expressed from an alternatively spliced transcript from the ZC3H11A/ZBED6 locus due to intron retention (Fig. 1*A*), showed a reduction in protein (Fig. 1*D*) and mRNA expression (Fig. 1*E*) similar to what would be expected for normal cellular genes. To our surprise, HAdV-5 growth in KO cells resulted in a drastic reduction in the production of most late viral capsid proteins (Fig. 1*F*), suggesting that ZC3H11A is required for optimal HAdV-5 replication. The decrease in capsid protein production also resulted in a threefold reduction in the formation of new infectious virus particles (Fig. 1*G*). In contrast, depletion of ZC3H11A had no or little effect on early HAdV5 gene expression, as demonstrated by the equal formation of viral replication centers (discussed below) containing the E2A-72K DNA-binding protein in WT and KO cells (Fig. S2).

ZC3H11A Deletion Impairs Growth of Multiple Nuclear-Replicating Human Viruses. To examine whether this host–virus interaction is unique to HAdV-5, we explored the effect of *ZC3H11A* KO on three additional nuclear-replicating viruses [HIV-1, influenza virus, and human herpes simplex virus 1 (HSV-1)] and two viruses with a cytoplasmic replication cycle [vaccinia virus Western Reserve strain (VV) and Semliki Forest virus (SFV)]. Infection of WT and KO HeLa cells with HIV-1 (strains IIIB and UG29A) indeed resulted in a significant reduction in HIV-1 virus production in the KO cells (Fig. 2*A*). To explore this effect on HIV-1 growth further, we transfected WT and ZC3H11A-KO cells with an HIV-1 reporter construct, NL4-3 ΔEnv Vpr luciferase reporter vector (pNL4-Luc) (13) (Fig. S3*A*). Measurement of Gag/pol and Tat mRNA expression by RT-PCR demonstrated that both were significantly reduced in KO cells compared with WT cells, whereas the control Renilla mRNA expression was not significantly affected by ZC3H11A inactivation (Fig. 2*B*). The reduction in Gag/pol mRNA expression was also manifested by reduced Gag protein expression (Fig. 2*C*). Further experiments demonstrated that growth of both influenza virus (H1N1 A/WSN/33 strain) and HSV-1 was also drastically reduced in KO cells, which is illustrated by a reduction in viral titers (Fig. 2 *D* and *E*) and viral protein production (Fig. 2 *F* and *G*). In contrast, VV and the SFV4 strain, which replicate in the cytoplasm, did not show any replication deficiency in the *ZC3H11A* KO cells (Fig. S3*B*). Collectively, our data suggest that ZC3H11A is required for efficient growth of several nuclear-replicating human viruses.

ZC3H11A Relocalizes to Viral Replication Centers in HAdV-5–Infected Cells. To gain insight into how ZC3H11A contributes to HAdV-5 infection, we analyzed ZC3H11A localization in both uninfected and HAdV-5–infected cells. Viral genomes are typically replicated and expressed in specific compartments in the cell. In the case of adenovirus, formation of these replication centers coincides with the start of viral DNA replication and the switch to the late phase of the infection. The replicating single-stranded viral DNA binds the E2A-72K DNA-binding protein and forms nuclear crescents or spheres that are surrounded by a ring-shaped zone where transcription and splicing take place (14). In uninfected cells, ZC3H11A is colocalized with the nuclear splicing speckle marker SRSF2 (alias human splice factor SC35) (Fig. 3*A*, *Left*). In contrast, in HAdV-5 late-infected cells, both ZC3H11A and SRSF2 are relocalized from nuclear speckles to nuclear foci, which are reminiscent of HAdV-5 replication centers (Fig. 3*A*, *Left*). To further study the localization of ZC3H11A, we generated a stable cell line (GFP-ZC3H11A) that was established by transfecting HeLa ZC3H11A-KO cells with a construct encoding a GFP-tagged ZC3H11A reporter construct under the transcriptional

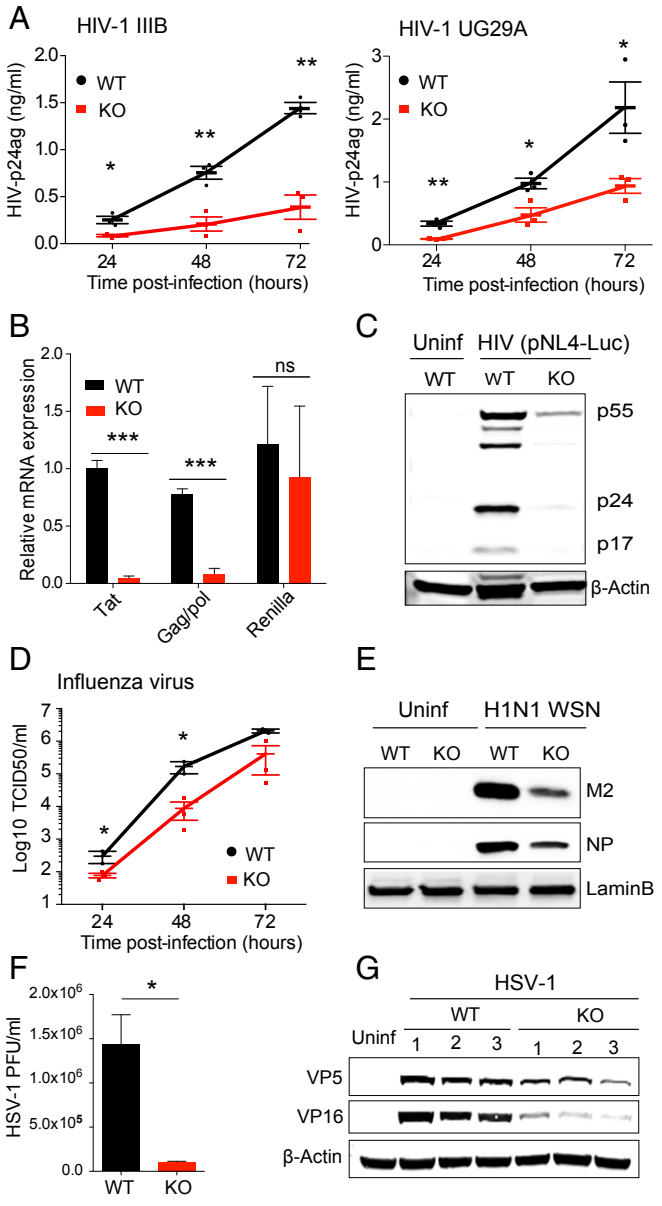

Fig. 2. ZC3H11A is required for efficient growth of nuclear-replicating viruses in HeLa cells. (*A*) Growth of HIV-1 IIIB (*Left*) and UG29A (*Right*) in WT (black) and ZC3H11A-KO (red) cells was measured using an HIV-1 p24 capture enzyme-linked immune assay. (*B*) Quantitative PCR quantification of HIV mRNA expression in WT (black) and ZC3H11A-KO (red) cells. (*C*) Expression of the HIV Gag protein (full-length P55 and processed forms P17 and P24) in WT and ZC3H11A-KO cells. (*D*) Viral titers (mean ± SEM) of H1N1 strain A/WSN/33 virus in WT (black) and ZC3H11A-KO (red) cells were determined using the $TCID_{50}$ method ($n = 3$). (*E*) Immunoblot against H1N1 M2 and NP in WT and ZC3H11A-KO cells using LaminB as a loading control. (*F*) HSV-1 titer in WT and ZC3H11A-KO cells. (*G*) Immunoblot against HSV-1 VP5 and VP16 in WT and ZC3H11A-KO cells using β-Actin as a loading control. $^*P < 0.05$, $^{**}P < 0.01$, $^{***}P < 0.001$; Student's *t* test. ns, not significant; PFU, plaque forming unit; Uninf, uninfected cells subjected to the same treatment as infected cells.

control of a CMV promoter. The GFP-ZC3H11A protein was shown to be functionally active as it could rescue the defective transport of adenovirus transcripts observed in ZC3H11A-KO cells (Fig. S4). During an adenovirus infection, ZC3H11A accumulates in a region surrounding the punctuate site of viral single-stranded DNA visualized using the viral E2A-72K DNA-binding protein (Fig. 3*A*, *Right*). Since this region is the site of active viral transcription and splicing, the results imply that ZC3H11A takes part in the processing of viral transcripts.

ZC3H11A Is an RNA-Binding Protein That Interacts with Purine-Rich Sequences. ZC3H11A was identified as one of 860 detected RNA-binding proteins in HeLa cells in a previous large-scale proteomic study (15). To study the RNA-binding properties of ZC3H11A in more detail, we performed UV cross-linking followed by ZC3H11A immunoprecipitation (CLIP) and RNaseI treatment to isolate the RNA protected by ZC3H11A (Fig. S5*A*). High-throughput sequencing (HITS) of the RNA isolated by CLIP revealed an almost exclusive interaction between ZC3H11A and protein-coding mRNAs in both uninfected and HAdV-5–infected cells (Fig. S5*B*). ZC3H11A binding showed a clear enrichment at coding exons and at the 3′ UTR of the mRNAs (Fig. S5*C*). Gene ontology (GO) analysis of ZC3H11A endogenous target mRNAs in the HAdV-5 HITS-CLIP data showed a significant enrichment of genes involved in mRNA metabolic processes, mRNA splicing, cellular response to stress, and the viral life cycle (Fig. S5*D*).

Interestingly, the cellular mRNAs targeted by ZC3H11A changed significantly between uninfected and HAdV-5–infected cells (Fig. 3*B*). As many as 37% and 43% of the cellular mRNAs showed exclusive binding to ZC3H11A in HAdV-5–infected cells or uninfected cells, respectively, whereas 20% of the mRNAs were targeted in both infected and uninfected cells (Dataset S1). This is well illustrated by the binding of ZC3H11A to the *NEAT1* and *RAN* mRNAs in uninfected versus HAdV-5–infected cells (Fig. 3*C*). In uninfected cells, ZC3H11A bound efficiently at the 3′ end of the paraspeckle *NEAT1* transcript, a binding that was almost completely lost in HAdV-5–infected cells. In contrast, ZC3H11A binding to the mRNA for the import and export factor RAN showed the reverse specificity, with an efficient binding only detectable in HAdV-5–infected cells. The ZC3H11A binding was restricted to only a few of the *RAN* exons. The effects of a HAdV-5 infection on the expression levels of *NEAT1* and *RAN* were modest compared with the changes in the HITS-CLIP data (Fig. S5*E*). The preferred binding motif for ZC3H11A shifted in HAdV-5–infected cells. In uninfected cells, ZC3H11A was found to bind to short purine-rich sequences, whereas the preferred binding motifs in HAdV-5–infected cells were more complex (Fig. 3*D*).

RNA-sequencing (RNA-seq) analysis of cytoplasmic mRNA showed around 1,650 differentially expressed (DE) genes between uninfected WT and KO cells (Fig. S6*A*). The GO analysis of DE genes revealed an enrichment of genes involved in RNA synthesis and RNA metabolism (Fig. S6*B*).

To investigate whether the ZC3H11A zinc finger domains were important for localization and function, we generated a mutant GFP-ZC3H11A expression construct lacking the three zinc finger domains ZC3H11A(ZFΔ3). An mRNA-binding protein capture assay demonstrated that the ZC3H11A(ZFΔ3) protein lacks RNA-binding capacity (Fig. 3*E*). ZC3H11A(ZFΔ3) was also redistributed from the speckle-like structures seen with the WT protein to an even distribution in the nucleus (Fig. 3*F*). Further, the ZC3H11A(ZFΔ3) protein was not able to rescue the defect in mRNA export in ZC3H11A-KO cells as revealed using an HIV-1–based luciferase reporter system (Fig. 3*G*), suggesting that the zinc fingers are critical for ZC3H11A function.

ZC3H11A Is Required for Efficient Viral mRNA Export. To study the effect of ZC3H11A on viral mRNA export, we performed an RNA-seq analysis of HAdV-5 mRNA expression in WT versus KO cells. We focused our analysis on the fiber mRNA for three reasons. First, previous studies have shown that among all of the viral late mRNAs, the fiber mRNA is subjected to the tightest export regulation (16, 17). Second, fiber protein accumulation

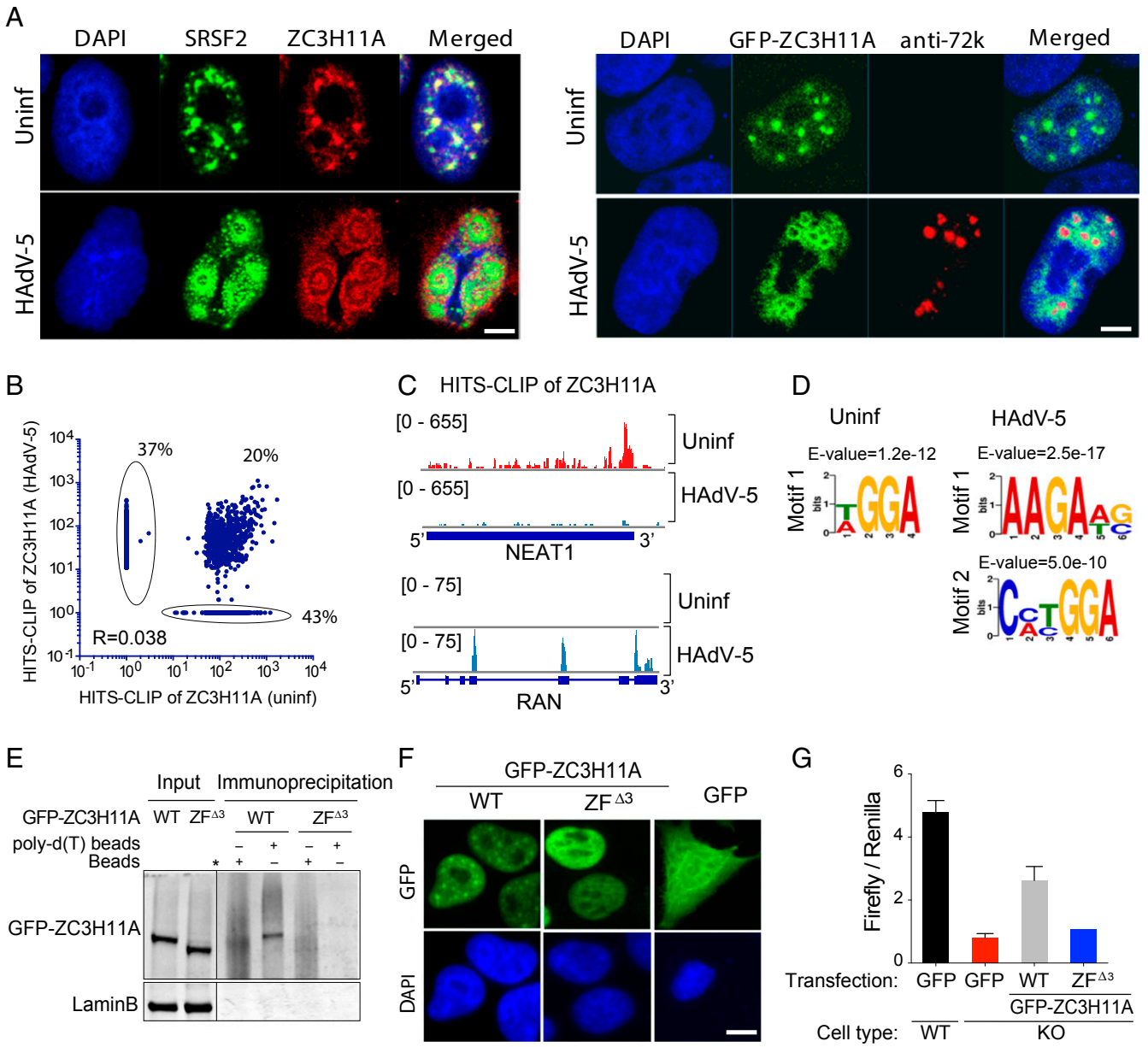

Fig. 3. Cellular localization of ZC3H11A and distribution of ZC3H11A HITS-CLIP targets before and after infection in HeLa cells. (*A*, *Left*) Immunofluorescence staining of WT cells using anti-ZC3H11A and anti-SRSF2 antibodies before and after infection with HAdV-5. (*A*, *Right*) Immunofluorescence staining with GFP-ZC3H11A and anti-72k protein antibody as a marker for HAdV-5 replication centers. (Scale bar: 5 μm.) (*B*) Correlation analysis of ZC3H11A target interactions in uninfected (Uninf) and infected cells based on HITS-CLIP, with a cutoff of 10 or more counts in Uninf or HAdV-5–infected samples. $R^2 = 0.04$, $P < 0.0001$. (*C*) Mapped reads over the *NEAT1* and *RAN* genes visualizing the ZC3H11A HITS-CLIP peaks in Uninf (red) and HAdV-5–infected (blue) cells. (*D*) Predicted motif for ZC3H11A binding in Uninf and HAdV-5–infected cells. (*E*) mRNA-binding proteins were pulled down using Dynabeads [oligo(dT)25] or Dynabeads protein G from cells transfected with plasmids expressing GFP-ZC3H11A (WT) or a truncated GFP-ZC3H11A lacking the three zinc finger domains ($ZF^{\Delta 3}$), followed by Western blotting using a GFP-specific antibody. The vertical black line shows the border between the two blots used to prepare this figure. (*F*) Localization of full-length GFP-ZC3H11A (WT) and the zinc finger mutant ($ZF^{\Delta 3}$) GFP was determined using a fluorescence microscope (*Top*) and nuclear DNA by DAPI staining (*Bottom*). (Scale bar: 10 μm.) (*G*) Luciferase activity of an HIV (pNL4-Luc) replicon in WT versus ZC3H11A-KO cells transfected with plasmids encoding the WT GFP-ZC3H11A protein or the GFP-ZC3H11A protein lacking zinc fingers ($ZF^{\Delta 3}$). A GFP-expressing plasmid construct was used as a control. A Renilla-expressing plasmid was cotransfected as a control for transfection efficiency.

was drastically reduced in KO cells, suggesting a regulation at the level of mRNA export (Fig. 1*F*). Third, the HITS-CLIP analysis revealed that ZC3H11A binds to most of the adenoviral transcript with a particularly strong interaction between ZC3H11A and the coding sequence of the HAdV-5 fiber mRNA (Fig. 4*A*). The abundance of gene expression was calculated as counts per million (cpm) reads. The RNA-seq data revealed that in WT cells, the fiber mRNA was more abundant in the cytoplasm (~60,000 cpm) than in total RNA (~40,000 cpm), suggesting a more efficient transport of the fiber mRNA compared with average transcripts (Fig. 4*B*, *Left*). In KO cells, fiber mRNA was down-regulated ~50% in the cytoplasm compared with WT cells, whereas the accumulation of hexon mRNA was essentially not affected by the absence of ZC3H11A (Fig. 4*B*). This result is consistent with the immunoblot data showing that all structural proteins, except hexon, are significantly reduced in ZC3H11A-KO cells (Fig. 1*F*).

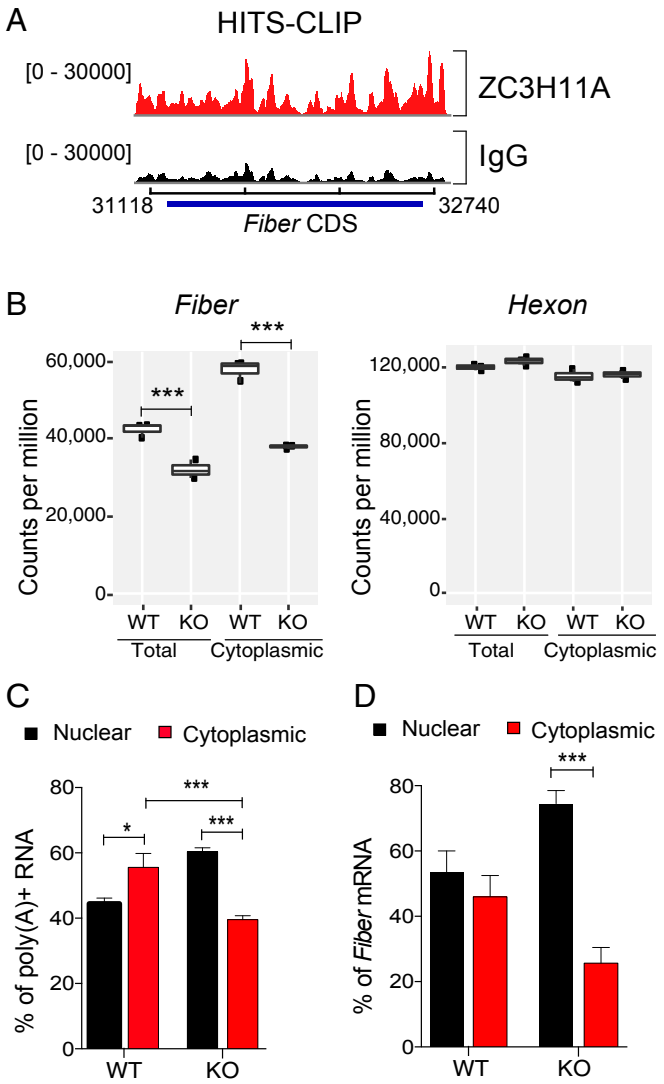

Fig. 4. ZC3H11A requirement for efficient viral mRNA export in HeLa cells. (*A*) ZC3H11A HITS-CLIP reads over the HAdV-5 fiber transcripts; the values to the left are the range of read counts, and the *x* axis shows the HAdV-5 genomic region spanning the fiber gene. (*B*) Counts (cpm) of RNA-seq reads of total and cytoplasmic adenovirus fiber and hexon mRNAs in WT and ZC3H11A-KO cells. (*C*) Quantification of RNA-FISH signal representing total poly(A)$^+$ transcripts. The result is presented as a percentage of total cellular mRNA accumulation in the nucleus and cytoplasm in WT and ZC3H11A-KO cells. (*D*) Quantification of the RNA-FISH signal detecting the fiber mRNA. Results represent the ratio of fiber mRNA accumulation in the nucleus and cytoplasm in WT and ZC3H11A-KO cells. ***$P < 0.001$, *$P < 0.05$.

FISH analysis of total poly(A)$^+$ RNA in uninfected cells showed that ZC3H11A inactivation resulted in a moderate decrease in total poly(A)$^+$ RNA accumulation in the cytoplasm (Fig. 4*C* and Fig. S7*A*). In contrast, RNA-FISH analysis of fiber mRNA accumulation in HAdV-5–infected cells showed a more dramatic decrease in mRNA export in KO cells (Fig. 4*D* and Fig. S7*B*). To further validate the result, we transfected ZC3H11A-KO cells with plasmids expressing GFP, GFP-ZC3H11A(WT), or GFP-ZC3H11A(ZFΔ3). The cytoplasmic accumulation of the fiber mRNA was enhanced in ZC3H11A-KO cells transfected with GFP-ZC3H11A(WT) plasmid but not with the backbone GFP plasmid or the GFP-ZC3H11A(ZFΔ3) mutant plasmid (Fig. S4). Results obtained using the pNL4-Luc HIV-1 reporter assay system, which expresses a measurable NEF-luciferase fusion protein (Fig. S3*A*), also demonstrated that the zinc finger domains are required for ZC3H11A to support mRNA export of HIV transcripts (Fig. 3*G*).

Taken together, our results show that the ZC3H11A protein is of critical importance for the export of at least a subset of the adenoviral and HIV-1 transcripts.

ZC3H11A Is a Heat Shock-Induced Protein. The increased amount of ZC3H11A during HAdV-5 infection (Fig. 1*D*) suggested that it might be a stress-induced protein. To test this possibility, we exposed HeLa-WT cells to heat shock (42 °C for 1 h), followed by a recovery period. As shown in Fig. 5*A* and quantitated in Fig. 5*B*, the heat shock treatment resulted in a twofold increase of ZC3H11A protein analogous to the increase of the classical heat shock protein HSP70. Similar to the results observed during HAdV-5 infection (Fig. 1*E*), the heat shock treatment did not result in a significant increase in *ZC3H11A* mRNA expression (Fig. 5*C*), suggesting that the increase in protein expression is a posttranscriptional event. In contrast to HSP70, which showed redistribution from the cytoplasm to the nucleus after heat shock (Fig. 5*D*), ZC3H11A showed nuclear localization before and after heat shock, with an increased concentration around the nucleoli after heat stress (Fig. 5*D*).

ZC3H11A is nonessential for HeLa cell growth under normal cell culture conditions (Fig. 1*C*). Since ZC3H11A is induced after heat shock, it might serve an important function under stress conditions. To test this, we compared the effect of heat shock on WT, ZC3H11A-KO, and KO cells expressing a stable GFP-ZC3H11A construct. We observed a small but significant reduction in cell viability in KO cells compared with WT cells, a cell viability that was partly rescued when ZC3H11A expression was restored in the GFP-ZC3H11A cells (Fig. 5*E*). Thus, ZC3H11A may have a role in maintaining cell functions during heat stress.

To further explore the regulation of ZC3H11A protein expression, we used the stable GFP-ZC3H11A cell line described above (Fig. 3*A*). Under normal growth conditions, the accumulation of the GFP-ZC3H11A protein was hardly detectable compared with the GFP protein expressed from the backbone plasmid (Fig. 5*F*, *Left*), suggesting that the GFP-ZC3H11A protein might be subjected to a rapid turnover. To test this possibility, we treated the GFP control and the GFP-ZC3H11A–expressing cell lines with the proteasome inhibitor MG132. MG132 treatment resulted in a significant increase in GFP-ZC3H11A protein accumulation, whereas the control cell line expressing GFP alone was largely unaffected (Fig. 5 *F* and *G*). Taken together, these results indicate that the increase in ZC3H11A protein expression under heat stress and during an adenovirus infection (Fig. 1*D*) might be regulated through a reduction in proteasomal degradation.

A previous large-scale proteomic screen showed that ZC3H11A is one of the proteins in the human proteome that shows the largest increase in small ubiquitin-like modifier (SUMO)-lyation (SUMOlyation) after heat stress and that ZC3H11A contains 10 putative SUMOlyation sites (18). Immunoblot analysis revealed that ZC3H11A shows a twofold increase in SUMOlyation after adenovirus infection (Fig. 5*H*). The results suggest that the increased protein abundance during stress could result from SUMOlyation-mediated protection of ZC3H11A from degradation.

Discussion

This study shows that the human ZC3H11A protein, which has been implicated as a component of the TREX complex (5, 6), is not essential for HeLa cell growth in tissue culture (Fig. 1*C*) but appears necessary for efficient growth of several nuclear-replicating viruses (Figs. 1*G* and 2). Thus, uninfected HeLa ZC3H11A-KO cells grow essentially as WT cells and display only a minor defect in export of cellular polyA$^+$ mRNAs (Fig. 4*C*). In contrast, export of the adenovirus fiber mRNA was severely reduced in the KO cells (Fig. 4*D*). Our study indicates that nuclear-replicating viruses

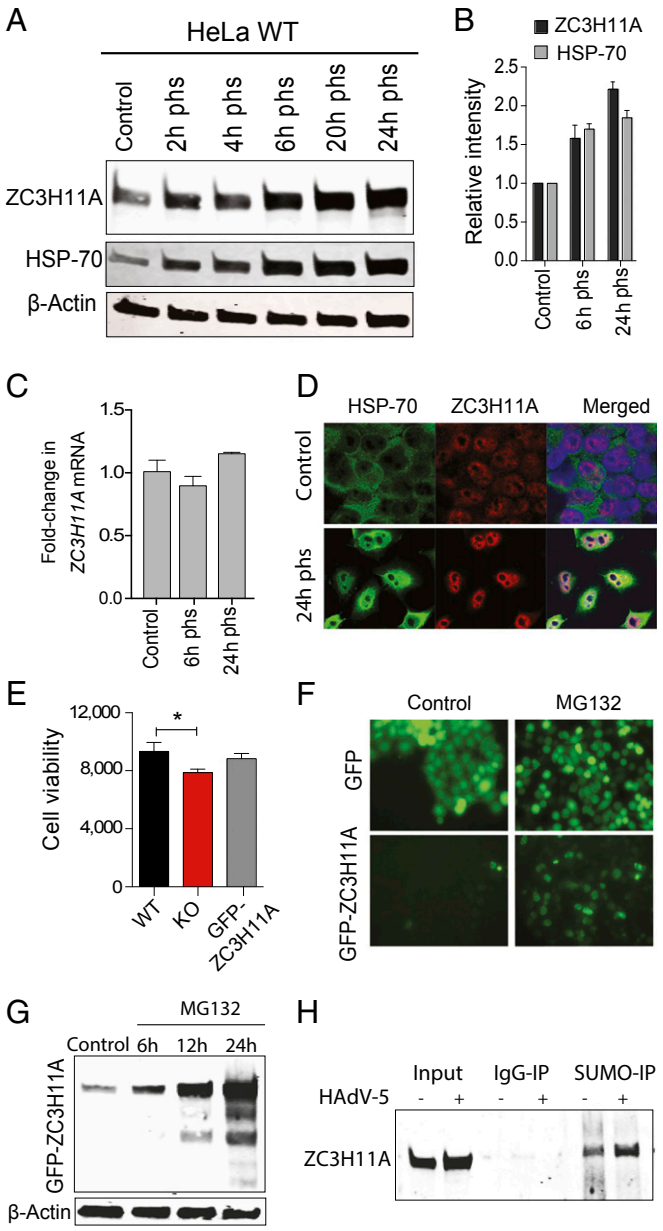

Fig. 5. ZC3H11A is a heat shock-induced nuclear protein. (*A*) Immunoblot detection of ZC3H11A, HSP70, and β-Actin after heat shock (42 °C for 1 h) in WT HeLa cells. (*B*) Bar plot illustrating band intensities of ZC3H11A and HSP70, normalized to β-Actin, at the indicated hours post-heat shock (phs). (*C*) Quantitative PCR analysis of *ZC3H11A* mRNA expression (mean ± SEM) before and after heat shock. (*D*) Immunofluorescence staining of ZC3H11A and HSP70 before and after heat stress. (*E*) Cell viability assay after heat shock. $*P < 0.05$. (*F*) Live cell imaging of ZC3H11A-KO cells stably expressing GFP (*Top*) or GFP-ZC3H11A (*Bottom*) in control cells and after 24 h of MG132 treatment. (*G*) Immunoblot detection of GFP-ZC3H11A after MG132 inhibition of the proteasome. (*H*) Immunoblot detection of ZC3H11A in uninfected and HAdV-5–infected HeLa WT cells after immunoprecipitation (IP) using anti-SUMO2/3 (SUMO-IP) and anti-IgG (IgG-IP).

"hijack" the ZC3H11A function to promote viral growth by facilitating export of viral mRNAs. However, it is noteworthy that most, but not all, HAdV-5 late mRNAs require ZC3H11A for efficient export (Fig. 4*B*), suggesting that there must be a specificity to ZC3H11A function that needs to be worked out.

ZC3H11A is a nuclear RNA-binding zinc finger protein that binds preferentially to purine-rich sequences (Fig. 3*D*). Splicing factor SRSF2 and ZC3H11A accumulate at nuclear speckles, also known as interchromatin granules, in uninfected cells and become redistributed to the viral replication centers in HAdV-5–infected cells. Mutating the three CCCH zinc fingers in ZC3H11A results in a failure to support HIV-1 and adenovirus cytoplasmic mRNA accumulation (Fig. 3*G* and Fig. S4) and the relocalization of ZC3H11A to nuclear splicing speckles (Fig. 3*F*). This reorganization of ZC3H11A and SRSF2 in HAdV-5–infected cells is consistent with previous studies, which have shown that nuclear bodies are reorganized in late-infected cells with a concentration of splicing factors at the diffuse ring-like structures active in transcription that surround the single-stranded DNA–containing centers (19–21). Continued progression of the infection results in the coalescence of viral gene expression sites and enlarged interchromatin granules that accumulate splicing factors, viral RNA, and late viral proteins. In late adenovirus-infected cells, export of host cell mRNA is blocked (22). Efficient export of late viral mRNAs requires the multifunctional adenovirus E4-ORF6/E1B-55K protein complex, which forms an E3 ubiquitin ligase complex together with cullin 5 and elongins B and C that, in addition to ubiquitinating p53 and Mre11, appears to ubiquitinate an unknown factor required for late mRNA export (23, 24). Interestingly, a recent proteomic search has identified the TREX complex components THOC2 and THOC5 as E1B-55K–associated proteins (25). It is attractive to speculate that the recruitment of ZC3H11A to the viral replication centers is part of the machinery that selectively exports newly transcribed viral mRNAs to the cytoplasm at the late phase of infection.

Our results suggest that ZC3H11A is a heat shock-induced protein that is subjected to posttranscriptional regulation at the level of protein stability. Thus, virus infection (Fig. 1*D*), heat stress (Fig. 5*A*), and inhibition of proteasome function (Fig. 5*G*) all resulted in a marked increase in the abundance of ZC3H11A without an increase in mRNA accumulation. Our data are compatible with a model where ZC3H11A serves a function to facilitate mRNA export, particularly under stress conditions, a function that nuclear-replicating viruses have hijacked to facilitate their own replication.

Multiple nuclear-replicating viruses, including adenovirus, influenza, hepatitis B, and herpes viruses, use the NXF1 mRNA export pathway for export of viral mRNAs to the cytoplasm (26–29). The TREX complex is typically recruited to mRNA through a process coupled to RNA splicing. Therefore, viral genes with introns have a more natural way to integrate to the NXF1 pathway. However, particularly the herpes family of viruses contains numerous genes without introns, and therefore uses viral adaptor proteins to enhance the recruitment of the TREX complex and NXF1 to such intronless mRNAs. The conserved ORF57 protein encoded by Kaposi's sarcoma-associated herpes virus is the best studied adaptor protein, recruiting ALYREF or the UIF factor (30, 31). ORF57 also recruits UAP56 and the remaining TREX complex components to the viral mRNAs to facilitate mRNA export. Other members of the herpes family of viruses encode proteins with a function homologous to Kaposi's sarcoma-associated herpes virus ORF57: herpes simplex virus ICP27 and herpes virus saimiri ORF57 (32), Epstein–Barr virus EB2 (33), and human cytomegalovirus UL69 (34). In addition to viral adaptor proteins, constitutive RNA transport elements that directly bind NXF1 with high affinity, and thereby promote export, have been identified in simple retroviruses, like Mason–Pfizer monkey virus (35).

The HIV-1 reverse (Rev) protein exports the unspliced genome (Gag/pol mRNA) and single-spliced mRNAs using the CRM1 export receptor, whereas double-spliced HIV-1 transcripts (Tat mRNA) use the NXF1 export pathway. In fact, Rev appears to be dominant and to suppress NXF1-dependent export by blocking recruitment of the TREX complex to the transcript (36). Since we observe a reduced cytoplasmic accumulation of both the Gag/pol and Tat mRNAs in ZC3H11A KO cells (Fig. 2*B*), our results indicate that ZC3H11A

may have a broader impact on multiple cellular RNA export machineries.

Clearly, viruses have evolved a number of different strategies to use the cellular mRNA export machineries to their own advantage. The present study shows that ZC3H11A is another host protein that is used for viral mRNA export during certain virus infections.

This study provides insight about host–pathogen interactions for several viruses of considerable medical importance. It reveals emerging opportunities for development of antiviral therapies based on interfering with the interaction between ZC3H11A and viral transcripts. ZC3H11A appears as an attractive drug target due to the mild phenotypic effects when this protein was knocked out in HeLa cells. Furthermore, the potential to exploit members of the TREX complex as targets for antiviral therapy is illustrated by the recent development of small-molecule inhibitors of the ATPase activity of the UAP56 protein, which effectively inhibited replication and virion production of human Kaposi's sarcoma-associated herpes virus (37).

Materials and Methods

Cell Culture. Human cervical carcinoma HeLa cells [American Type Culture Collection (ATCC) CCL-2] were maintained in Dulbecco's modified Eagle medium (DMEM) with 2 mM L-glutamine, 1 mM sodium pyruvate, and 4.5 g/L glucose (ATCC 30-2001), supplemented with 10% heat-inactivated FBS and penicillin (0.2 U/mL)/streptomycin (0.2 μg/mL)/L-glutamine (0.2 μg/mL) (Gibco) at 37 °C in a 5% CO_2 humidified atmosphere. Heat shock was induced by adding preheated medium (42 °C) to the cells, which were then incubated at 42 °C for 1 h.

Genome Editing. *ZC3H11A* was knocked out in HeLa cells using CRISPR/Cas9. A specific gRNA for *ZC3H11A* was designed using the CRISPRdirect tools (38). A gRNA expression cassette containing the U6 promoter, the gRNA, a gRNA scaffold, and a termination signal (39) was synthesized by Integrated DNA Technologies (Fig. S1*A*). JetPrime transfection reagent (Polyplus) was used to deliver the CRISPR/Cas9 reagents into HeLa cells, including the gRNA expression fragment, a linear hygromycin marker (Clontech), and a Cas9-expressing plasmid pSpCas9(BB)-2A-GFP (PX458; Addgene) (40). Transfected cells were kept under a selective medium for 2 wk. Single-cell clones were screened for *ZC3H11A* disruption using primers flanking the targeted site, followed by Sanger sequencing of individual clones.

Immunofluorescence Staining. Cells were cultured in an eight-well slide chamber (BD Falcon) overnight to around 60–70% confluence. The cells were washed with PBS and fixed with 4% paraformaldehyde for 10 min at room temperature. The fixed cells were permeabilized with 0.25% Triton X-100 and then blocked for nonspecific binding with 2% BSA in PBS. The primary antibodies (Table S1) were diluted in PBS containing 1% BSA and incubated with the cells overnight. Cells were washed three times with PBS and then incubated with Alexa Fluor-labeled secondary antibodies (Table S1). DAPI was used for counterstaining. Slides were analyzed using a confocal microscope (Zeiss LSM 700).

RNA-FISH. The mRNA transcripts were detected using an HPLC-purified oligo(dT) 70 probe labeled at the 5′ end with ATTO 590 NHS Ester. HeLa cells grown on a slide chamber were fixed with 4% formaldehyde for 10 min, rinsed three times with PBS, permeabilized with 0.5% Triton X-100 for 10 min at room temperature, and rinsed again with PBS. Cells were incubated with hybridization buffer [0.4 μM oligo(dT)70, 0.5 μg of transfer RNA (Ambion), 1% BSA, 10% (vol/vol) dextran sulfate, 50% deionized formamide, and 2× sodium saline citrate (SSC)] overnight at 37 °C in a humid chamber containing 50% deionized formamide. Thereafter, the cells were washed twice with 2× SSC, once with 0.5× SSC, and once with PBS. The immunofluorescence staining was performed as described above. The intensity of fluorescence signals was quantified using ImageJ (v1.50i; NIH). The fiber mRNA was detected using an HPLC-purified RNA probe (Fig. S7*C*) labeled at the 5′ end with ATTO 633 NHS Ester.

Real-Time Quantitative PCR. Total RNA was extracted from cells using an RNeasy Mini Kit (Qiagen), while cytoplasmic RNA was isolated using a PARIS Kit (ThermoFisher), and the samples were treated with DNase I. A High-Capacity cDNA Reverse Transcription Kit (Applied Biosystems) was used to generate cDNA from the extracted RNA. Quantitative PCR analysis was performed using ABI MicroAmp Optical 384-Well Reaction Plates on an ABI 7900 Fast Real-Time PCR System (Applied Biosystems). Forward and reverse primers (IDT) for each gene were mixed with SYBR Green Gene Expression Master Mix (Applied Biosystems) in a 10-μL total reaction volume. Primer sequences are listed in Table S2.

Immunoblot Analysis. Total protein lysates were prepared using radioimmunoprecipitation assay (RIPA) lysis buffer containing protease inhibitors (Complete Ultra Tablets; Roche). Equal amounts of total lysates were separated on a gradient SDS/PAGE (4–15%; Bio-Rad) and transferred to PVDF membranes (Millipore). StartingBlock buffer (Thermo Scientific) was used to block the membrane before the indicated primary and secondary antibodies were used for immunoblotting (Table S1). Proteins were visualized and detected by an Odyssey system (LI-COR).

Protein Immunoprecipitation. HeLa cells were washed once with 1× PBS, and total protein lysate was harvested using the RIPA buffer with sonication for five cycles (30 s each). Total protein lysate was immediately heated at 70 °C for 10 min, followed by centrifugation at 18,000 × *g* at 4 °C for 5 min. Cell lysates were incubated with the SUMO antibody (Table S1) or IgG (2 μg of antibody per 1 mL of lysate) coupled with Dynabeads Protein G (ThermoFisher) overnight at 4 °C. The beads were washed four times with RIPA buffer and finally mixed with 2× SDS sample buffer.

RNA-Seq. HeLa WT and ZC3H11A-KO cells, around 20 million, uninfected or infected with HAdV-5 [50 fluorescence-forming units (FFUs) per cell for 20 h] were washed in PBS, and total RNA was extracted using the RNeasy Mini Kit. The RNA quality and integrity were measured with an RNA ScreenTape assay (TapeStation; Agilent Technologies). Strand-specific mRNA-seq libraries were generated using a SENSE RNA-Seq Library Prep Kit (Lexogen) following the manufacturer's instructions. For each sample, 2 μg of total RNA was poly-A–selected using oligo(dT) beads to enrich for mRNA, and the RNA-seq libraries were amplified by 12 PCR cycles. The libraries were sequenced as 125-bp paired-end reads using Illumina HiSeq. Sequence reads were mapped to the reference human genome (hg19) using STAR 2.5.1b with default parameters. HTSeq 0.6.1 (Python package) was used to generate read counts, and edgeR (Bioconductor package) was used to identify DE genes using gene models for hg19 downloaded from the UCSC Gene Browser (www.genome.ucsc.edu). The abundance of gene expression was calculated as cpm reads. Genes with less than four cpm reads in at least three samples were filtered out. The filtered libraries were normalized using the trimmed mean of M-values normalization method (41). The corrected *P* value for multiple testing using the false discovery rate approach was used to determine the significance of DE genes. For GO analysis, the DE genes were submitted to ClueGO (42), a Cytoscape plug-in. All expressed genes were used as background, and the Biological Process and Kyoto Enclopedia of Genes and Genomes pathway tables were used to identify enriched GO terms. For the infected samples, we mapped the reads to the HAdV-5 reference genome (AC_000008.1) (https://www.ncbi.nlm.nih.gov/). The RNA-seq reads have been deposited in the Sequence Read Archive repository (https://www.ncbi.nlm.nih.gov/Traces/study/?acc=SRP133853) with the accession number SRP133853.

HITS-CLIP. HITS-CLIP was performed as described elsewhere (43), with the following modifications. Briefly, HeLa WT cells, around 20 million, uninfected or infected with HAdV-5 (50 FFUs per cell for 20 h) were washed twice with 1× PBS and then irradiated twice with 400 mJ/cm^2 at 254 nm, followed by cell lysis using RIPA buffer [supplemented with 2 U/mL DNase I and 10 μL/mL RNaseI (1:500 dilution)] with sonication for 10 cycles (30 s off and 30 s on). Cell lysates were incubated with 2.5 μg of ZC3H11A (human atlas) or IgG (Santa Cruz Biotechnology) antibodies with rotation overnight. The antibodies were captured with Dynabeads protein G for 40 min with rotation at room temperature. The beads were washed four times with RIPA buffer and once with dephosphorylation buffer [50 mM Tris (pH 7.9), 100 mM NaCl, 10 mM $MgCl_2$, 1 mM DTT] followed by calf intestinal phosphatase (New England Biolabs) treatment as described in the manufacturer's manual. After that, the beads were washed twice in phosphatase wash buffer [50 mM Tris (pH 7.9), 20 mM EDTA, 0.5% Np40)] and once with PNK buffer [50 mM Tris (pH 7.9), 50 mM NaCl, 10 mM MgCl)]. The 5′-end of the bound RNA was labeled with T4 polynucleotide kinase (New England Biolabs) by adding 0.5 μL of ^{32}P γ-ATP (total reaction volume pf 50 μL) for 30 min at 37 °C, followed by cold chase incubation for 30 min after addition of 0.75 μL of 10 mM ATP. The beads were washed four times with PNK buffer. Finally, the beads were mixed thoroughly with 2× Laemmli loading dye and separated on SDS/PAGE, followed by transfer to PVDF membranes. The membranes were subjected to autoradiography, and bands corresponding to the size of ZC3H11A and above were cut from both the ZC3H11A and IgG lanes. RNA was extracted from the membrane by proteinase K digestion, phenol extrac-

tion, and ethanol precipitation. Illumina RNA-seq libraries were prepared from the purified RNA using the NEXTflex Small RNA-Seq Kit (BIOO Scientific). The libraries were sequenced as 50-bp single reads using the HiSeq high-output mode.

Raw sequence reads were trimmed using Cutadapt (44) and mapped to the reference human genome (hg19) or HAdV-5 reference genome (AC_000008.1) using STAR 2.5.1b (45), setting the multimapper to 1. For cellular HITS-CLIP analysis, a genomic feature count was done using BEDtools Multicov (46), and we discarded genomic features with less than 10-fold more counts in the ZC3H11A-HITS-CLIP library versus the IgG ZC3H11A-HITS-CLIP library. Analysis of the distribution of transcript types (e.g., protein coding, pseudogene, small nucleolar RNA) of ZC3H11A-HITS-CLIP target transcripts was done using HTSeq (47). Genome-wide distribution of ZC3H11A-HITS-CLIP reads across the gene body was assessed using the read distribution tool of RSeQC suite (48). ZC3H11A-specific filtered reads were submitted to PIPE-CLIP (49) to define HITS-CLIP peaks. Top peaks were selected based on peak width for an uninfected sample cutoff of 150 nt (average peak width of 80 nt) and for an HAdV-5–infected sample cutoff of 90 nt (average peak width of 38 nt). Top peak-corresponding reads were extracted after putative duplicate reads had been deleted, and were then used for predicting enriched motifs in ZC3H11A-bound RNA using the MEME suite (50). The CLIP-seq reads have been submitted to the short reads archive (https://www.ncbi.nlm.nih.gov/Traces/study/?acc=SRP133853) with the accession number SRP133853.

mRNA-Binding Protein Capture Assay. The mRNA-binding protein capture assay was adapted from Castello et al. (51). Briefly ∼48 h posttransfection, around 20 million HeLa cells transfected with plasmids expressing GFP-ZC3H11A (WT) or a truncated GFP-ZC3H11A ($ZF^{\Delta 3}$) were washed twice with 1× PBS and then irradiated twice with 400 mJ/cm^2 at 254 nm, followed by cell lysis using RIPA buffer (supplemented with 2 units of DNase I per milliliter) with sonication for 10 cycles (30 s off and 30 s on). Cell lysates were incubated with either Dynabeads [oligo(dT)25] or Dynabeads protein G overnight, with rotation at 4 °C. The beads were washed four times with RIPA buffer, followed by Western blotting using a GFP-specific antibody.

Generation of ZC3H11A-KO Clones with Restored Expression of *ZC3H11A*. The coding sequences of *ZC3H11A* were cloned into AcGFP1C1 vector (Clontech). HeLa ZC3H11A-KO cells were transfected with an AcGFP-ZC3H11A fusion construct and kept under selective medium with G418. Pure single-cell expression clones were obtained after 2 wk of selection. As a control, AcGFP1-expressing ZC3H11A-KO HeLa cells were also generated. Control and stably transfected cells were used in the previously indicated experiments. The GFP-ZC3H11A construct lacking zinc fingers ($ZF^{\Delta 3}$) was generated by deleting the DNA sequence segment encoding for the three zinc finger domains.

Virus Infection. Infection of adherent cells by HAdV-5 or HVS-1 was done as previously described (52). Adenovirus titers were measured as FFUs (53) using a pan-hexon antibody (MAB8052, 1:500 dilution; Millipore). Herpes simplex type 1 virus titer was measured by a plaque assay.

To monitor influenza replication, equal cell densities of the three different ZC3H11A-KO clones and the parental HeLa cell line were infected with the H1N1 strain A/WSN/33 and cultured in infection media [DMEM with 0.1% FBS, 0.3% BSA, 10 U/mL penicillin and streptomycin, and 2.5 mg/mL tosyl phenylalanyl chloromethyl ketone (TPCK)-treated trypsin]. At the indicated times postinfection, equal aliquots of culture medium were removed and clarified by centrifugation at 1,000 × *g* for 5 min, and the resulting viral titers were determined by the median tissue culture infectious dose ($TCID_{50}$) method using MDCK cells as previously described (54).

WT VV and SFV4 were propagated and titrated in HeLa and BHK-21 cells, respectively. Both viruses were purified by sucrose density ultracentrifugation. Monolayer WT or ZC3H11A-KO HeLa cells cultured in six-well plates were incubated with VV or SFV4 for 2 h with 500 μL of medium. The cells were then washed and overlaid with 2 mL of cell culture medium supplied with 0.6% carboxymethyl cellulose (semisolid format to restrict virus particle spread). The infected cell cultures were kept in culture, and formed plaques were visualized 4–5 d later using crystal violet staining.

To study the effect on HIV replication, HeLa WT and ZC3H11A-KO cells were cultured in RPMI 1640 supplemented with 10% FCS, 10 IU/mL penicillin, and 50 μg/mL streptomycin. The HIV-1 IIIB/MuLV and HIV-1 92UG29/MuLV pseudovirus stocks (55) were prepared as described elsewhere (56), and were used to infect 70–80% confluent HeLa cells cultured in 24-well cell culture plates at 37 °C in 5% CO_2/air. Three concentrations of clade B HIV-1 IIIB/MuLV pseudovirus (1,000, 100, and 20 $TCID_{50}$) and two virus concentrations of HIV-1 clade A 92UG29/MuLV pseudovirus (500 and 50 $TCID_{50}$) were added in triplicate wells per virus concentration, and kept for 2 h at 37 °C in 5% CO_2/air. The cells were washed three times with RPMI 1640 medium and then incubated at 37 °C in 5% CO_2/air for up to 72 h. Medium was collected after 24, 48, and 72 h. The content of HIV-1 p24 antigen in the culture medium was quantitatively measured in an HIV-1 p24 capture enzyme-linked immune assay (57). In short, plates of 96 wells were coated with a polyclonal rabbit anti-p24 antibody (7.5 μg/mL). Standards used for HIV-1 p24 antigen (0.033 to 4 ng/mL; Protein Sciences) and cell supernatants from virus cultures treated with 0.5% Triton X-100 to disrupt virus particles were added to the plate (100 μL per well) in duplicate wells per sample and incubated overnight. After washing, an HRP-labeled murine anti–HIV-1 p24 mAb was added for 2 h. After washing, *o*-phenylene diamine substrate (100 μL per well) was added. The color reaction was developed by the orthophenylene diamine and (H_2O_2) peroxidase substrate and measured as OD at 492 nm.

Luciferase Assay. HeLa WT or ZC3H11A-KO cells were transfected with the reporter plasmid pNL4-3.Luc.R^-.E^- (referred to here as pNL4-Luc) (13). The luciferase assay was performed 24 h posttransfection with the Dual-Luciferase Reporter Assay System (Promega) according to the manufacturer's instructions. Both firefly and Renilla luciferase activity was measured with an Infinite M200 luminometer (Tecan). The results were presented as a normalized ratio of firefly to Renilla and were based on means from at least three biological replicates. The statistical analysis comprised a two-tailed unpaired *t* test and was performed using Prism6 (GraphPad Software). A P value <0.05 was considered statistically significant.

Cell Growth Measurements. WT cells and cells from three ZC3H11A-KO clones (10,000 cells per line) were seeded in 24-well plates in growth media and cultured for 7 d with real-time measurement of cell density every 12 h using an IncuCyte instrument (Essen Bioscience).

Cell Viability Assay. Cells were seeded in 24-well plates (30,000 cells per well) and allowed to attach. One day later, the cells were placed in growth media at 42 °C for 1 h, followed by an incubation at 37 °C for 2 h to recover. Cells were incubated for 1 h with growth media containing 10% PrestoBlue (Invitrogen). The reduction of PrestoBlue reagent was measured on a Tecan Sunrise Plate Reader with the following parameters: bottom-read fluorescence (excitation = 560 nm, emission = 590 nm).

Additional information is available in *Supporting Information*.

ACKNOWLEDGMENTS. We thank Ali Sheikari for excellent support with cell cultures. The following reagent was obtained through the NIH AIDS Reagent Program, Division of AIDS, National Institute of Allergy and Infectious Diseases, NIH: pNL4-3.Luc.R^-.E^- from Dr. Nathaniel Landau. This project was supported by the Knut and Alice Wallenberg Foundation and the Swedish Cancer Society. Computer resources were supplied by Uppsala Multidisciplinary Center for Advanced Computational Science (UPPMAX).

1. Van Laere AS, et al. (2003) A regulatory mutation in *IGF2* causes a major QTL effect on muscle growth in the pig. *Nature* 425:832–836.
2. Markljung E, et al. (2009) ZBED6, a novel transcription factor derived from a domesticated DNA transposon regulates IGF2 expression and muscle growth. *PLoS Biol* 7:e1000256.
3. Younis S, et al. (2018) The ZBED6-IGF2 axis has a major effect on growth of skeletal muscle and internal organs in placental mammals. *Proc Natl Acad Sci USA* 115:E2048–E2057.
4. Liang J, Song W, Tromp G, Kolattukudy PE, Fu M (2008) Genome-wide survey and expression profiling of CCCH-zinc finger family reveals a functional module in macrophage activation. *PLoS One* 3:e2880.
5. Dufu K, et al. (2010) ATP is required for interactions between UAP56 and two conserved mRNA export proteins, Aly and CIP29, to assemble the TREX complex. *Genes Dev* 24:2043–2053.
6. Hein MY, et al. (2015) A human interactome in three quantitative dimensions organized by stoichiometries and abundances. *Cell* 163:712–723.
7. Wickramasinghe VO, Laskey RA (2015) Control of mammalian gene expression by selective mRNA export. *Nat Rev Mol Cell Biol* 16:431–442.
8. Heath CG, Viphakone N, Wilson SA (2016) The role of TREX in gene expression and disease. *Biochem J* 473:2911–2935.
9. Cheng H, et al. (2006) Human mRNA export machinery recruited to the 5′ end of mRNA. *Cell* 127:1389–1400.
10. Masuda S, et al. (2005) Recruitment of the human TREX complex to mRNA during splicing. *Genes Dev* 19:1512–1517.
11. Folco EG, Lee C-S, Dufu K, Yamazaki T, Reed R (2012) The proteins PDIP3 and ZC11A associate with the human TREX complex in an ATP-dependent manner and function in mRNA export. *PLoS One* 7:e43804.
12. Beltz GA, Flint S (1979) Inhibition of HeLa cell protein synthesis during adenovirus infection: Restriction of cellular messenger RNA sequences to the nucleus. *J Mol Biol* 131:353–373.

13. Connor RI, Chen BK, Choe S, Landau NR (1995) Vpr is required for efficient replication of human immunodeficiency virus type-1 in mononuclear phagocytes. *Virology* 206:935–944.
14. Schmid M, Speiseder T, Dobner T, Gonzalez RA (2014) DNA virus replication compartments. *J Virol* 88:1404–1420.
15. Castello A, et al. (2012) Insights into RNA biology from an atlas of mammalian mRNA-binding proteins. *Cell* 149:1393–1406.
16. Pilder S, Moore M, Logan J, Shenk T (1986) The adenovirus E1B-55K transforming polypeptide modulates transport or cytoplasmic stabilization of viral and host cell mRNAs. *Mol Cell Biol* 6:470–476.
17. Gonzalez R, Huang W, Finnen R, Bragg C, Flint SJ (2006) Adenovirus E1B 55-kilodalton protein is required for both regulation of mRNA export and efficient entry into the late phase of infection in normal human fibroblasts. *J Virol* 80:964–974.
18. Hendriks IA, et al. (2014) Uncovering global SUMOylation signaling networks in a site-specific manner. *Nat Struct Mol Biol* 21:927–936.
19. Aspegren A, Rabino C, Bridge E (1998) Organization of splicing factors in adenovirus-infected cells reflects changes in gene expression during the early to late phase transition. *Exp Cell Res* 245:203–213.
20. Bridge E, Pettersson U (1996) Nuclear organization of adenovirus RNA biogenesis. *Exp Cell Res* 229:233–239.
21. Pombo A, Ferreira J, Bridge E, Carmo-Fonseca M (1994) Adenovirus replication and transcription sites are spatially separated in the nucleus of infected cells. *EMBO J* 13:5075–5085.
22. Flint SJ, Gonzalez RA (2003) Regulation of mRNA production by the adenoviral E1B 55-kDa and E4 Orf6 proteins. *Curr Top Microbiol Immunol* 272:287–330.
23. Blanchette P, et al. (2008) Control of mRNA export by adenovirus E4orf6 and E1B55K proteins during productive infection requires E4orf6 ubiquitin ligase activity. *J Virol* 82:2642–2651.
24. Woo JL, Berk AJ (2007) Adenovirus ubiquitin-protein ligase stimulates viral late mRNA nuclear export. *J Virol* 81:575–587.
25. Hung G, Flint SJ (2017) Normal human cell proteins that interact with the adenovirus type 5 E1B 55kDa protein. *Virology* 504:12–24.
26. Read EK, Digard P (2010) Individual influenza A virus mRNAs show differential dependence on cellular NXF1/TAP for their nuclear export. *J Gen Virol* 91:1290–1301.
27. Yatherajam G, Huang W, Flint SJ (2011) Export of adenoviral late mRNA from the nucleus requires the Nxf1/Tap export receptor. *J Virol* 85:1429–1438.
28. Yang CC, Huang EY, Li HC, Su PY, Shih C (2014) Nuclear export of human hepatitis B virus core protein and pregenomic RNA depends on the cellular NXF1-p15 machinery. *PLoS One* 9:e106683.
29. Larsen S, et al. (2014) Influenza polymerase encoding mRNAs utilize atypical mRNA nuclear export. *Virol J* 11:154.
30. Boyne JR, Colgan KJ, Whitehouse A (2008) Recruitment of the complete hTREX complex is required for Kaposi's sarcoma-associated herpesvirus intronless mRNA nuclear export and virus replication. *PLoS Pathog* 4:e1000194.
31. Malik P, Blackbourn DJ, Clements JB (2004) The evolutionarily conserved Kaposi's sarcoma-associated herpesvirus ORF57 protein interacts with REF protein and acts as an RNA export factor. *J Biol Chem* 279:33001–33011.
32. Tunnicliffe RB, et al. (2011) Structural basis for the recognition of cellular mRNA export factor REF by herpes viral proteins HSV-1 ICP27 and HVS ORF57. *PLoS Pathog* 7: e1001244.
33. Hiriart E, et al. (2003) A novel nuclear export signal and a REF interaction domain both promote mRNA export by the Epstein-Barr virus EB2 protein. *J Biol Chem* 278: 335–342.
34. Lischka P, Toth Z, Thomas M, Mueller R, Stamminger T (2006) The UL69 transactivator protein of human cytomegalovirus interacts with DEXD/H-box RNA helicase UAP56 to promote cytoplasmic accumulation of unspliced RNA. *Mol Cell Biol* 26:1631–1643.
35. Kang Y, Bogerd HP, Cullen BR (2000) Analysis of cellular factors that mediate nuclear export of RNAs bearing the Mason-Pfizer monkey virus constitutive transport element. *J Virol* 74:5863–5871.
36. Taniguchi I, Mabuchi N, Ohno M (2014) HIV-1 Rev protein specifies the viral RNA export pathway by suppressing TAP/NXF1 recruitment. *Nucleic Acids Res* 42: 6645–6658.
37. Schumann S, et al. (2016) Targeting the ATP-dependent formation of herpesvirus ribonucleoprotein particle assembly as an antiviral approach. *Nat Microbiol* 2:16201.
38. Naito Y, Hino K, Bono H, Ui-Tei K (2015) CRISPRdirect: Software for designing CRISPR/Cas guide RNA with reduced off-target sites. *Bioinformatics* 31:1120–1123.
39. Mali P, et al. (2013) RNA-guided human genome engineering via Cas9. *Science* 339: 823–826.
40. Ran FA, et al. (2013) Genome engineering using the CRISPR-Cas9 system. *Nat Protoc* 8: 2281–2308.
41. Robinson MD, Oshlack A (2010) A scaling normalization method for differential expression analysis of RNA-seq data. *Genome Biol* 11:R25.
42. Bindea G, et al. (2009) ClueGO: A Cytoscape plug-in to decipher functionally grouped gene ontology and pathway annotation networks. *Bioinformatics* 25:1091–1093.
43. Grozdanov PN, MacDonald CC (2014) High-throughput sequencing of RNA isolated by cross-linking and immunoprecipitation (HITS-CLIP) to determine sites of binding of CstF-64 on nascent RNAs. *Polyadenylation: Methods and Protocols*, eds Rorbach J, Bobrowicz AJ (Humana Press, Totowa, NJ), pp 187–208.
44. Martin M (2011) Cutadapt removes adapter sequences from high-throughput sequencing reads. *EMBnet J* 17:10–12.
45. Dobin A, et al. (2013) STAR: Ultrafast universal RNA-seq aligner. *Bioinformatics* 29: 15–21.
46. Quinlan AR (2014) BEDTools: The Swiss-Army tool for genome feature analysis. *Current Protocols in Bioinformatics* 47:11.12.1–11.12.34.
47. Anders S, Pyl PT, Huber W (2015) HTSeq–A Python framework to work with high-throughput sequencing data. *Bioinformatics* 31:166–169.
48. Wang L, Wang S, Li W (2012) RSeQC: Quality control of RNA-seq experiments. *Bioinformatics* 28:2184–2185.
49. Chen B, Yun J, Kim MS, Mendell JT, Xie Y (2014) PIPE-CLIP: A comprehensive online tool for CLIP-seq data analysis. *Genome Biol* 15:R18.
50. Bailey TL, et al. (2009) MEME SUITE: Tools for motif discovery and searching. *Nucleic Acids Res* 37:W202–W208.
51. Castello A, et al. (2013) System-wide identification of RNA-binding proteins by interactome capture. *Nat Protoc* 8:491–500.
52. Kamel W, Segerman B, Öberg D, Punga T, Akusjärvi G (2013) The adenovirus VA RNA-derived miRNAs are not essential for lytic virus growth in tissue culture cells. *Nucleic Acids Res* 41:4802–4812.
53. Philipson L (1961) Adenovirus assay by the fluorescent cell-counting procedure. *Virology* 15:263–268.
54. da Silva DV, et al. (2015) The influenza virus neuraminidase protein transmembrane and head domains have coevolved. *J Virol* 89:1094–1104.
55. Ljungberg K, Rollman E, Eriksson L, Hinkula J, Wahren B (2002) Enhanced immune responses after DNA vaccination with combined envelope genes from different HIV-1 subtypes. *Virology* 302:44–57.
56. Andäng M, et al. (1999) Dose-response resistance to HIV-1/MuLV pseudotype virus ex vivo in a hairpin ribozyme transgenic mouse model. *Proc Natl Acad Sci USA* 96: 12749–12753.
57. Devito C, Levi M, Broliden K, Hinkula J (2000) Mapping of B-cell epitopes in rabbits immunised with various gag antigens for the production of HIV-1 gag capture ELISA reagents. *J Immunol Methods* 238:69–80.